

# ROLE OF FEEDBACK IN AGN-HOST COEVOLUTION: A STUDY FROM PARTIALLY OBSCURED ACTIVE GALACTIC NUCLEI

J. Wang

*National Astronomical Observatories, Chinese Academy of Sciences, 20A, Datun Road, Chaoyang District, Beijing, China, 100012*

---

## Abstract

Partially obscured AGNs within a redshift range  $z = 0.011 \sim 0.256$  are used to re-study the role of feedback in the AGN-host coevolution issue in terms of their [OIII] $\lambda 5007$  emission line profile. The spectra of these objects enable us to determine the AGN's accretion properties directly from their broad  $H\alpha$  emission. This is essential for getting rid of the "circular reasoning" in our previous study of narrow emission-line galaxies, in which the [OIII] emission line was used not only as a proxy of AGN's bolometric luminosity, but also as a diagnostic of outflow. In addition, the measurement of  $D_n(4000)$  index is improved by removing an underlying AGN's continuum according to the corresponding broad  $H\alpha$  emission. With these improvements, we confirm and reinforce the correlation between  $L/L_{\text{Edd}}$  and stellar population age. More important is that this correlation is found to be related to both [OIII] line blue asymmetry and bulk blueshift velocity, which suggests a linkage between SMBH growth and host star formation through the feedback process. The current sample of partially obscured AGNs shows that the composite galaxies have younger host stellar population, higher Eddington ratio, less significant [OIII] blue wing and smaller bulk [OIII] line shift than do the Seyfert galaxies.

*Keywords:*

galaxies: nuclei - galaxies: evolution - quasars: emission line

---

## 1. INTRODUCTION

Although the nature is still not fully understood at present, active galactic nuclei (AGNs) are widely believed to co-evolve with their host galaxies (see Kormendy & Ho 2013 for a recent review). The concept of co-evolution mainly stems from two observational facts: 1) the tight correlations between the mass of the central supermassive blackhole (SMBH) and several properties of the bulge of the host galaxy, including the velocity dispersion, luminosity and mass of the bulge (e.g., Magorrian et al. 1998; Gebhardt et al. 2000; Merritt & Ferrarese 2001; McLure & Dunlop 2002; Tremaine et al. 2002; Haring & Rix 2004; Ferrarese & Ford 2005; Aller &

---

\*Corresponding author

Email address: wj@bao.ac.cn (J. Wang)

Preprint submitted to New Astronomy

November 18, 2014

Richstone 2007; Gultekin et al. 2009; Woo et al. 2010); 2) both AGN’s accretion and star formation have a peak at similar redshifts of  $z = 2 \sim 3$ . (e.g., Ueda et al. 2003; Croom et al. 2004; Hasinger et al. 2005; Nandra et al. 2005; Silverman et al. 2008; Shankar et al. 2009; Aird et al. 2010; Assef et al. 2011).

What is associated with the gas fall onto a SMBH is the AGN’s feedback that results in an interaction between the energy released in the accretion and the gas in the host galaxy (see a review in Fabian 2012). In the local universe, a kpc-scale outflow has been frequently identified by spatially resolved spectroscopy for both ionized (e.g., Holt et al. 2008; Fu & Stockton 2009; Rupke & Veilleux 2011; Westmoquette et al. 2011) and molecular (e.g., Feruglio et al. 2010; Alatalo et al. 2011) gas. Recent observations point out that the interstellar medium (ISM) throughout the host can be photoionized and kinematically disturbed by AGN’s feedback (e.g., Fu & Stockton 2009; Greene et al. 2011). In fact, involving a feedback is useful for solving the “over cooling” problem in the  $\Lambda$  cold dark matter ( $\Lambda$ CDM) galaxy formation model in which the predicted massive galaxies are much more numerous than the observed ones (e.g., Ciotti & Ostriker 2007; Somerville et al. 2008; Hirschmann et al. 2013), and for reproducing the observed  $M - \sigma_*$  relation, luminosity functions of quasars and normal galaxies (e.g., Haehnelt et al. 1998; Silk & Rees 1998; Fabian 1999; Kauffmann & Haehnelt 2000; Granato et al. 2004; Springel et al. 2005; Di Matteo et al. 2005, 2007; Croton et al. 2006; Hopkins et al. 2007, 2008; Khalatyan et al. 2008; Menci et al. 2008; Somerville et al. 2008; Power et al. 2011; Scannapieco et al. 2012). Dehnen & King (2013) recently proposed a new scenario of SMBH growth in which the SMBH accretion disk is formed because of the feedback. The gas that is swept-up by the feedback finally falls towards the SMBH on near-parabolic orbit when the feedback weakens.

It has been known for a long time that a large fraction of [OIII] doublet show blue asymmetry and bulk blueshift with respect to the systemic velocity (e.g., Heckman et al. 1981; Veron-Cetty et al. 2001; Zamanov et al. 2002; Marziani et al. 2003; Aoki et al. 2005; Bian et al. 2005; Boroson 2005; Komossa et al. 2008; Xu & Komossa 2009; Zhang et al. 2013). The observed [OIII] line profile is generally explained by an interaction between NLR clouds and wind from central AGNs, which is supported by the spatially resolved spectroscopic observations of a few nearby Seyfert 2 galaxies, although the origin of the wind is still an open issue. The observations carried out with Hubble Space Telescope indicate a NLR kinematics with a radial outflow acceleration of form  $v = kr$  at a radius  $r < r_t$  and a deceleration of  $v = v_{max} - kr$  beyond the turnover radius  $r_t$  (e.g., Fischer et al. 2013 and references therein).

By using the two dimensionless shape parameters (i.e., skewness and kurtosis) to quantify the [OIII] $\lambda$ 5007 line shape deviation from a pure Gaussian function in narrow emission-line galaxies, Wang et al. (2011) indicate a trend that AGNs with stronger blue asymmetries tend to be associated with younger stellar populations. The authors additionally argued that the trend is likely driven by the co-evolution between AGN’s Eddington ratio ( $L/L_{Edd}$ , where  $L_{Edd} = 1.26 \times 10^{38} (M_{BH}/M_\odot) \text{ erg s}^{-1}$  is the Eddington luminosity) and host galaxy, when  $L([OIII])/\sigma_*^4$  is used as a proxy of  $L/L_{Edd}$ . The argument is mainly based upon the correlation between  $L([OIII])/\sigma_*^4$  and line skewness. However, it is generally accepted that a combination of a narrow core Gaussian profile and an additional blueshifted, broad Gaussian component is required to reproduce an observed asymmetric [OIII] $\lambda$ 5007 line profile. There is therefore a circular argument on which the measured  $L([OIII])$  contains the contributions from both components.

In order to avoid the “circular reasoning” issue, this paper re-studies the evolution of [OIII] line profile by focusing on partially obscured AGNs that are excluded in our previous study.

Here, the partially obscured AGNs refer to Seyfert 1.8/1.9 galaxies and composite galaxies<sup>1</sup> with a Seyfert 1.8/1.9-like spectrum. In addition to the [OIII] line profile and host stellar population, the spectra of these objects allow us to directly estimate  $L/L_{\text{Edd}}$  from their broad H $\alpha$  emission. The partially obscured AGNs are excluded in Wang et al. (2011) because of the contamination from the central AGN's continuum, which generally results in an underestimation of the modeled stellar population age. In this paper, the underestimation is alleviated by properly removing the underlying AGN's continuum from each observed spectrum.

The paper is organized as follows. The sample selection and spectral analysis are presented in Section 2 and Section 3, respectively. The results are shown in Section 4, and the implications are discussed in Section 5. A  $\Lambda$ CDM cosmology with parameters  $H_0 = 70 \text{ km s}^{-1} \text{ Mpc}^{-1}$ ,  $\Omega_m = 0.3$ , and  $\Omega_\Lambda = 0.7$  (Spergel et al. 2003) is adopted throughout the paper.

## 2. PARTIALLY OBSCURED AGNS FROM MPA/JHU SDSS DR7 CATALOG

A sub-sample of partially obscured AGNs has already been identified by Wang et al. (2011) from the value-added SDSS Data Release 7 (Abazajian et al. 2009) Max-Planck Institute for Astrophysics/Johns Hopkins University (MPA/JHU) catalog (see Heckman & Kauffmann 2006 for a review). The sample totally contains 229 broad-line Seyfert galaxies/LINERs and broad-line composite galaxies after removing the duplicates. Their redshifts range from 0.0111 to 0.025. We refer the readers to Section 2 and 3.4 in Wang et al. (2011) for the details of the sample selection. Briefly, the sample requires: 1) a spectrum has a median signal-to-noise ratio (S/N) per pixel of the whole spectrum  $S/N > 20$  (number of entries: 135,912); 2) all the emission lines used in the traditional Baldwin-Phillips-Terlevich (BPT) diagnostic diagram (e.g., Veilleux & Osterbrock 1987) are detected with a significance level of at least  $3\sigma$  (number of entries: 39,384). 3) the [OIII] $\lambda$ 5007 emission line has  $S/N > 30$  (number of entries: 10,913); 4) the [OIII] line width has  $\sigma_{\text{obs}} > 2\sigma_{\text{inst}}$ , where  $\sigma_{\text{inst}} = 65 \text{ km s}^{-1}$  is the instrumental resolution of the SDSS spectroscopic survey (number of entries: 3,478); 5) redshift does not lie within the range from 0.11 to 0.12<sup>2</sup> (number of entries after removing the duplicates: 2,616); 6) a broad H $\alpha$  component can be identified in the spectrum by means of its blue high-velocity wing after the stellar features are removed from the spectrum. The broad component is automatically selected by the criterion  $F_w/\sigma_c \geq 3$ , where  $F_w$  is the specific flux of the line wing averaged within the wavelength range from 6500 to 6350 Å in the rest frame and  $\sigma_c$  the standard deviation of the continuum flux within the emission-line-free region ranging from  $\lambda$ 5980 to  $\lambda$ 6020.

## 3. SPECTRAL ANALYSIS

The 1-Dimensional spectra of the partially obscured AGNs are analyzed by the IRAF<sup>3</sup> package. The spectral analysis includes Galactic extinction correction, transformation to the rest

<sup>1</sup>A galaxy is classified as a composite one if it is located in the [OIII]/H $\beta$  versus [NII]/H $\alpha$  diagnostic diagram between the empirical and theoretical demarcation lines that separate AGNs from star-forming galaxies. See Section 4.1 for the details.

<sup>2</sup>This is useful for excluding the possible fake spectral profile caused by the poorly subtracted strong sky emission line [OI] $\lambda$ 5577 at the observer frame.

<sup>3</sup>IRAF is distributed by National Optical Astronomy Observatory, which is operated by the Association of Universities for Research in Astronomy, Inc., under cooperative agreement with the National Science Foundation.

frame, starlight component removal and emission line profile measurement. The Galactic extinction is corrected for each spectrum by the color excess  $E(B - V)$  taken from the Schlegel, Finkbeiner, and Davies Galactic reddening map (Schlegel et al. 1998), by assuming an  $R_V = 3.1$  extinction law of the MilkyWay (Cardelli et al. 1989). The spectrum is then **shifted to the rest frame using** the redshift provided by the SDSS pipelines. The reduced spectrum in the rest-frame of a partially obscured AGN SDSS J095156.71+023602.0 is shown in Figure 1 as an illustration.

### 3.1. Stellar Features Removal and Stellar Population

The continuum of the partially obscured AGNs is dominated by the starlight component emitted from the host galaxies. We model the stellar absorption features from each rest-frame spectrum as the sum of the first seven eigenspectra. The eigenspectra are built through the principal component analysis (PCA) method (e.g., Francis et al. 1992; Hao et al. 2005; Wang & Wei 2008) from the standard single stellar population spectral library developed by Bruzual & Charlot (2003). A Galactic extinction curve with  $R_V = 3.1$  is adopted in the modeling to account for the intrinsic extinction due to the host galaxy. A  $\chi^2$  minimization is performed for each of the spectra over the rest-frame wavelength range from 3700 to 8000Å, except for the regions with strong emission lines. The modeling and subtraction of the starlight component is illustrated in Figure 1 for SDSS J095156.71+023602.0.

The modeled starlight component is used to measure host stellar population age. The 4000Å break index  $D_n(4000)$  (Bruzual 1983; Balogh et al. 1999) defined as

$$D_n(4000) = \frac{\int_{4000}^{4100} f_\lambda d\lambda}{\int_{3850}^{3950} f_\lambda d\lambda} \quad (1)$$

is generally used as an excellent mean age indicator of the stellar population of the bulge of a galaxy until a few Gyr after the onset of a star formation activity (e.g., Kauffmann et al. 2003; Heckman et al. 2004;; Kewley et al. 2006; Kauffmann & Heckman 2009; Wild et al. 2007, 2010; Wang & Wei 2008, 2010; Wang et al. 2011, 2013).

The contamination due to the underlying AGN's continuum is an issue and must be considered in the stellar population synthesis of partially obscured AGNs. The observed broad H $\alpha$  emission demonstrates the existence of an underlying AGN's continuum leaking from the edge of the torus according to the unified model (e.g., Antonucci 1993). The leaking powerlaw continuum impacts the spectral shape at the blue end, which always results in an underestimate of  $D_n(4000)$  index, and consequently a relatively younger stellar population if the contamination is ignored (e.g., Cid Fernandes & Terlevich 1995; Storchi-Bergmann et al. 2000; Cid Fernandes et al. 2004; Wang et al. 2013). Strictly speaking, the best way to remove the underlying AGN's continuum is to model the observed continuum by a linear combination of a power-law continuum and the used eigenspectra. This is, however, a hard task according to our experiments because of the strong degeneracy between the AGN's continuum and the blue spectra of hot stars. The degeneracy typically results in a significant overestimate of the amplitude of the powerlaw component (e.g., Cid Fernandes et al. 2004; Wang et al. 2013).

An alternative approach is adopted here to remove the underlying AGN's continuum. A scaled powerlaw (i.e.,  $f_\lambda \propto \lambda^{-\alpha}$ ) is subtracted from each modeled starlight spectrum that is dereddened by the modeled local extinction in advance. The amplitude of the powerlaw is estimated from the tight  $L_{5100\text{Å}}-L_{\text{H}\alpha}$  relation (Eq. 4). The relation finally yields a specific flux of the powerlaw

at 5100Å:  $f_{5100\text{Å}} \approx 10^{-3}\beta f_{\text{H}\alpha}$ , where  $f_{\text{H}\alpha}$  is the measured line flux of broad H $\alpha$  emission, and  $\beta$  accounts for the effect on the flux due to reddening.

We at first checked the effect of different powerlaw index  $\alpha$  on the measured  $D_n(4000)$  value. The variation of powerlaw shape accounts for not only the intrinsic scatter of  $\alpha$  around its typical value of 1.7 (e.g., Vanden Berk et al. 2001 and references therein), but also the uncertainty due to reddening of AGN's continuum. When  $\alpha$  varies from 1.5 to 1.9, a tiny change  $\leq 0.02$  can be obtained for  $D_n(4000)$ , which is significantly smaller than the dynamical range ( $\sim 1.0$ ) of the measured  $D_n(4000)$ . This result is not unreasonable because the specific flux ratio between the two powerlaws with  $\alpha = 1.5$  and 1.9 has a shape  $\propto \lambda^{-0.4}$ , which is very close to a flat spectrum within the narrow wavelength ranges defining  $D_n(4000)$ .

The left panel in Figure 2 compares the  $D_n(4000)$  index measured with the powerlaw correction ( $[\alpha, \beta] = [1.7, 1.0]$ ) with that without the correction. One can see clearly from the comparison: 1) as expected, an enhancement of  $D_n(4000)$  value after the correction of powerlaw; 2) the enhancement moderately increases with the measured  $D_n(4000)$ . The increase could be understood as follows. In a spectrum with larger 4000Å break, the relative flux level contributed by a powerlaw has a more significant difference between the wavelength ranges blueward and redward of 4000Å. The right panel shows the same comparison but in the case of  $[\alpha, \beta] = [1.7, 2.0]^4$ . As expected, a stronger AGN's continuum results in a larger  $D_n(4000)$  enhancement and a more significant increasing of the enhancement with  $D_n(4000)$  value. Moreover, a larger scatter could be seen from the comparison for a stronger AGN's continuum.

Without a further statement, the  $D_n(4000)$  value measured after the powerlaw correction with  $[\alpha, \beta] = [1.7, 1.0]$  is used throughout the subsequent analysis. The effect on the results by different powerlaw level is discussed in Section 5.2.

### 3.2. Emission Line Measurement

After the removal of the starlight component, the emission-line profiles are at first modeled by the SPECFIT task (Kriss 1994) in the IRAF package in the emission-line isolated spectra for both H $\alpha$  and H $\beta$  regions<sup>5</sup>. Each line is modeled by a linear combination of a set of several Gaussian profiles. The intensity ratios of the [OIII] and [NII] doublets are fixed to their theoretical values. The flux of the [OI] $\lambda$ 6300 emission line is measured through direct integration by the SPLIT task in the IRAF package.

By following the method in Wang et al. (2011), the two high-order line shape parameters  $\xi_3$  (Skewness) and  $\xi_4$  (kurtosis) are used to quantify the line shape deviation from a pure Gaussian profile (Binney & Merrifield 1998). The parameters are defined as  $\xi_k = \mu_k / \sigma^k$  ( $k = 3, 4$ ), where

$$\mu_k = \left(\frac{c}{\bar{\lambda}}\right)^k \frac{\int (\lambda - \bar{\lambda})^k f_\lambda d\lambda}{\int f_\lambda d\lambda} \quad (2)$$

is the  $k$ -order moment of line and  $\sigma$  the second-order moment in units of  $\text{km s}^{-1}$  (i.e.,  $k = 2$  in Eq. 2).  $f_\lambda$  is the specific flux density of the continuum-subtracted emission line, and  $\bar{\lambda} =$

<sup>4</sup>A factor of  $\beta = 2$  is used by taking into account of the factor of  $f_e \sim 0.47$  obtained in Wang & Wei (2008). The factor  $f_e$  represents an upper limit on the reducing of broad H $\alpha$  lines emission due to reddening.

<sup>5</sup>These spectral modelings are performed for the two reasons. At first, an integrated narrow-line flux is required for the subsequent examination in the Baldwin-Phillips-Terlevich (BPT, Baldwin et al. 1981; Veilleux & Osterbrock 1987) diagrams. Secondly, the broad H $\alpha$  component is required to be separated from the observed line profile for the estimation of both SMBH accretion properties and level of the underlying AGN's continuum.

$\int \lambda f_\lambda d\lambda / \int f_\lambda d\lambda$  the line centroid (i.e., the first moment) of the emission line. A value of  $\xi_3 > 0$  corresponds to a red asymmetry, and  $\xi_3 < 0$  a blue asymmetry. The emission line with a value of  $\xi_4 > 3$  has a peak profile superposed on a broad base, while the line with  $\xi_4 < 3$  has a boxy line profile<sup>6</sup>. Figure 3 presents the  $\xi_3$  versus  $\xi_4$  diagram for the partially obscured AGNs. The figure shows a sequence starting from the pure Gaussian region (i.e.,  $\xi_3 = 0$ ,  $\xi_4 = 3$ ) to the upper left corner for both Seyfert and transition galaxies with broad Balmer emission, which is highly consistent with that in Wang et al. (2011) for narrow emission-line galaxies.

The [OIII] $\lambda$ 5007 line bulk relative velocity shift is calculated as  $\Delta v = c\Delta\lambda/\lambda_0$ , where  $\lambda_0$  and  $\Delta\lambda$  are the rest-frame wavelength of the [OIII] $\lambda$ 5007 emission line and the wavelength shift with respect to the narrow H $\beta$  line, respectively. The narrow H $\beta$  line shows a very small velocity shift relative to the galaxy rest frame (e.g., Komossa et al. 2008).  $\Delta v$  is based on the measured line centroids ( $\bar{\lambda}$ ) and on the wavelengths in a vacuum of both H $\beta$  and [OIII] lines. The calculated  $\Delta v$  is compared with the  $\xi_3$  (the left panel) and  $\xi_4$  (the right panel) parameters in Figure 4. The trends plotted in the two diagrams are very close to that for narrow emission-line galaxies shown in Wang et al. (2011). A spearman rank-order test yields a correlation between  $\Delta v$  and  $\xi_3$  with a correlation coefficient of  $r_s = 0.439$  and a probability of null correlation of  $P = 1.8 \times 10^{-11}$  corresponding to a Z-value of 4.53. One can see from the left panel that there is a small fraction of the objects that deviate from the correlation at the large blueshift end. The right panel indicates that these objects are dominated by the “boxy”, rather than the peaked, [OIII] line profiles, which is again in agreement with that in Wang et al. (2011). The authors have argued that a boxy line profile could be reproduced by the sum of two or more (distinct) peaks with comparable fluxes and line widths, which results in a shift of line centroid.

### 3.3. Deriving Physical Properties of Accretion

The two basic parameters (i.e.,  $L/L_{\text{Edd}}$  and  $M_{\text{BH}}$ , where  $L_{\text{Edd}} = 1.26 \times 10^{38} M_{\text{BH}}/M_\odot$ ) of SMBH accretion are estimated from the AGN’s broad H $\alpha$  line emission that is obtained through our spectral profile modeling. Greene & Ho (2007) provided an updated estimator of the mass of central SMBH

$$M_{\text{BH}} = (3.0^{+0.6}_{-0.5}) \times 10^6 \left( \frac{L_{\text{H}\alpha}}{10^{42} \text{ ergs s}^{-1}} \right)^{0.45 \pm 0.03} \left[ \frac{\text{FWHM}(\text{H}\alpha)}{10^3 \text{ km s}^{-1}} \right]^{2.06 \pm 0.06} M_\odot \quad (3)$$

by combining the revised luminosity-radius relation (with a scatter of 30-50% of the measured radius) reported in Bentz et al. (2006) and the  $L_{5100\text{\AA}}$ - $L_{\text{H}\alpha}$  relation in Greene & Ho (2005)

$$L_{5100\text{\AA}} = 2.4 \times 10^{43} \left( \frac{L_{\text{H}\alpha}}{10^{42} \text{ ergs s}^{-1}} \right)^{0.86} \text{ ergs s}^{-1} \quad (4)$$

where  $L_{\text{H}\alpha}$  is the intrinsic luminosity of the H $\alpha$  broad component corrected for local extinction. The luminosity relation has a rms scatter around the best-fit line of 0.2dex. The extinction is obtained from the narrow-line ratio H $\alpha$ /H $\beta$  for each object, assuming the Balmer decrement for standard case B recombination and a Galactic extinction curve with  $R_V = 3.1$ . The AGN’s bolometric luminosity is then derived from the calibration  $L = 9\lambda L_\lambda(5100\text{\AA})$  (Kaspi et al. 2000).

<sup>6</sup>We refer the readers to Section 3.5 in Wang et al. (2011) for the uncertainties of the skewness and kurtosis parameters of  $\Delta\xi_3 = 0.14$  and  $\Delta\xi_4 = 0.20$  that are derived from the duplicate observations. We emphasize that the sample selection in the current study is the same as that in Wang et al. (2011), except for the broad H $\alpha$  emission.

## 4. ANALYSIS AND RESULTS

This section presents the statistical study on the partially obscured AGNs based on the spectral measurements described above. The spectral properties of these objects enable us to determine the AGN’s accretion properties directly from their broad  $H\alpha$  emission instead of from other proxy. This is essential for getting rid of the “circular reasoning” in our previous study of narrow emission-line galaxies (Wang et al. 2011). In that study, both bolometric luminosity of AGN and line profile parameters are derived from  $[\text{OIII}]\lambda 5007$  emission line. In total, 15 objects are excluded from the subsequent statistical analysis either because of their poor starlight removal or because of their poor S/N of the broad  $H\alpha$  emission.

### 4.1. BPT Diagnostic Diagrams

Figure 5 displays the three BPT diagrams for the final 170 broad-line Seyfert galaxies and 44 broad-line transition galaxies<sup>7</sup>. All the line ratios are calculated from the narrow Balmer line emission that is obtained through our profile modeling. The  $[\text{OIII}]\lambda 5007$  line flux used in the line ratio calculation is the sum of both narrow and broad (mostly blueshifted) components because these two components are required to properly model the observed  $[\text{OIII}]$  line profile. The diagrams are a powerful tool in determining the dominant powering source in narrow emission-line galaxies through their emission-line ratios. The solid lines in the three panels show the theoretical demarcation lines separating “pure” AGNs from star-forming galaxies (Kewley et al. 2001). The long-dashed and dotted line in the left panel mark the empirical demarcation line proposed in Kauffmann et al. (2003) and the theoretical one proposed by Stasinska et al. (2006), respectively. Based upon their new photoionization models, Stasinska et al. (2006) claimed that their demarcation line is slightly restrictive in separating “pure” starforming galaxies than the empirical one. As shown by the diagrams, almost all the objects listed in the sample are located above these demarcation lines, and our sample is strongly biased against LINERs that are typical of low  $[\text{OIII}]/H\beta$  ratio. The bias is caused by our sample selection that requires a high S/N ratio (and consequently a large flux) of  $[\text{OIII}]$  emission line.

### 4.2. $[\text{OIII}]$ Line Profile Versus Stellar Population

The measured  $D_n(4000)$  value is plotted against  $\xi_3$  (the left panel) and  $\Delta\nu$  (the right panel) in Figure 6. At first, the diagrams confirm the results obtained in the previous studies (e.g., Kewley et al. 2006; Schawinski et al. 2007; Wang & Wei 2008; Wang et al. 2011): the transition galaxies are clustered in the region with younger stellar populations than do Seyfert galaxies, which implies that the transition galaxies are at an intermediate evolutionary phase in the context of the co-evolution of AGNs and their host galaxies (see discussion and references in Wang et al. 2011). Secondly, although no evident correlation can be identified from the two diagrams, a clear difference can be obtained if the sample is separated into two parts according to their stellar population ages. The separation is marked by a dashed line with  $D_n(4000) = 1.5$  in each panel. This value is usually used to define young/old stellar population according to the  $D_n(4000)$  measurement (e.g., Kauffmann et al. 2003). The partially obscured AGNs associated with young stellar populations show a wide range in their  $[\text{OIII}]$  line profiles that vary from a

<sup>7</sup> Among these 214 partially obscured AGNs, there are 29 common objects listed in the *ROSAT*-SDSS-DR5 catalog that is originally crossmatched by Anderson et al. (2007). Their rest-frame X-ray luminosities in the 0.1-2.4 keV band range from  $10^{42}$  to  $10^{44} \text{ erg s}^{-1}$ . This range indicates that some of these objects are AGNs (e.g., those having a luminosity above  $10^{43} \text{ erg s}^{-1}$ ).

blue asymmetrical shape to a Gaussian function. On the contrary, a symmetric line profile is typical for the AGNs associated with old stellar populations. A similar trend can be also found in the  $\Delta\nu$  case. AGNs with significant [OIII] blueshift ( $\Delta\nu < 150\text{km s}^{-1}$ ) can be only observed in the galaxies with young stellar populations with  $D_n(4000) < 1.4$ .

#### 4.3. $L/L_{\text{Edd}}$ Derived From Broad $H\alpha$ Emission

The left panel in Figure 7 plots  $L/L_{\text{Edd}}$  as a function of stellar population age. A significant correlation can be identified between AGN's accretion power and host galaxy stellar population age: larger the  $L/L_{\text{Edd}}$ , younger the host stellar population will be ( $r_s = -0.622$ ,  $P = 3.1 \times 10^{-27}$  and  $Z = 6.72$  for the Spearman rank-order test). The strong correlation confirms and reinforces the results that obtained by many authors in the previous studies (see discussion for more details). We parametrize the relationship as the best fit of

$$\log L/L_{\text{Edd}} = -1.75 - 2.88x + 4.08x^2 \quad (5)$$

where  $x = 1/D_n(4000)$ , The relationship is over plotted by a dashed line in the diagram.

$L/L_{\text{Edd}}$  is plotted against  $\xi_3$  in the middle panel of Figure 7. Similar as the  $D_n(4000)$  versus  $\xi_3$  diagram, there is no evident relationship between the two parameters at first glance. However, one can identify a trend that the objects are avoid to occupy the left-bottom corner with low  $L/L_{\text{Edd}}$  and strong [OIII] blue asymmetry. To reveal this trend more clearly, we separate the sample into two parts basing upon  $\xi_3 = -0.5$ . Figure 8 compares the distributions of  $L/L_{\text{Edd}}$  of the two sub-samples. When compared with the AGNs with weaker [OIII] blue asymmetry, the distribution of the ones with stronger asymmetry is slightly shifted towards the higher  $L/L_{\text{Edd}}$  end. A two-sided Kolmogorov-Smirnov test yields a marginal difference between the two distributions at a significance level of  $P = 0.95$  with a maximum absolute discrepancy of 0.23 in logarithm. Mullaney et al. (2013) compares the stacking [OIII] line profiles with various AGN's parameters for 24,264 optically selected AGNs. Their panel b in Figure 3 indicates a trend in which the strength of the [OIII] blue wing increases with Eddington ratio, which is consistent with the result reported here.

The right panel in Figure 7 presents an anti-correlation between  $L/L_{\text{Edd}}$  and  $\Delta\nu$ , which is failed to be identified for narrow emission-line galaxies in Wang et al. (2011). The correlation indicates that the bulk velocity blueshift of [OIII] emission line increases with  $L/L_{\text{Edd}}$ . A Spearman rank-order test returns a correlation coefficient  $r_s = -0.319$  at a significance level of  $P = 1.9 \times 10^{-6}$  ( $Z = 3.29$ ). Zhang et al. (2011) recently analyzed a large and homogeneous sample of radio-quiet Seyfert 1 galaxies and quasars selected from SDSS. Their analysis indicates that the bulk velocity shift of [OIII] is found to be strongly related with  $L/L_{\text{Edd}}$ : the large velocity shift generally occurs in the AGNs with high  $L/L_{\text{Edd}}$  (see also in e.g., Boroson 2005; Bian et al. 2005). As a rare population, the “blue outliers” are the objects with strong [OIII] blueshifts larger than  $250\text{ km s}^{-1}$  (e.g., Zamanov et al. 2002; Zhou et al. 2006). Spectroscopic observations point out that these objects occupy the high  $L/L_{\text{Edd}}$  end in the Eigenvector-I (EI) space, and are exclusively Population A objects<sup>8</sup> that have small broad  $H\beta$  line widths ( $< 4000\text{ km s}^{-1}$ ) and strong FeII complex emission (e.g., Zamanov et al. 2002; Marziani et al. 2003; Komossa et al. 2008; Marziani & Sulentic 2012).

<sup>8</sup>AGNs are separated into **two populations, A (having  $\text{FWHM}(H\beta) < 4000\text{ km s}^{-1}$  and large RFe) and B (having  $\text{FWHM}(H\beta) > 4000\text{ km s}^{-1}$  and small RFe)**, where RFe is defined as the FeII to broad  $H\beta$  line ratio. Generally speaking, **Population A AGNs have higher  $L/L_{\text{Edd}}$  than do Population B AGNs (see citations in the main text)**. Population A AGNs contain Narrow-line Seyfert 1 galaxies that are believed to be at early evolution stage (e.g., Mathur 2000).



Compared with the Seyfert galaxies, one can learn from Figure 7 that the composite galaxies in the current sample have extreme properties with younger host stellar population, higher Eddington ratio, less significant [OIII] blue wing and smaller bulk [OIII] line shift.

## 5. DISCUSSION

### 5.1. An Underestimation and Bias of $L/L_{\text{Edd}}$

As discussed in Wang & Wei (2008), although  $L_{\text{H}\alpha}$  is an acceptable measurement of the accretion power in partially obscured AGNs, a systematical underestimate of  $L/L_{\text{Edd}}$  and  $M_{\text{BH}}$  can not be avoided both because of the obscuration of the torus and because of the reddening in the broad-line region. Our previous study obtained an upper limit of underestimate of  $\sim 50\%$  for  $L/L_{\text{Edd}}$  and  $\sim 70\%$  for  $M_{\text{BH}}$ .

The underestimate of  $L_{\text{H}\alpha}$  could be learned in the left panel of Figure 9, which compares the distribution of  $L_{\text{H}\alpha}$  between the used partially obscured AGNs and typical type I AGNs in Greene & Ho (2007)<sup>9</sup>. The difference between the peaks of the two distributions is about 0.5 dex. This difference is likely caused by the reddening and obscuration of the broad H $\alpha$  emission. The middle panel compares the calculated  $M_{\text{BH}}$  between the two samples. A strong bias against small  $M_{\text{BH}}$  could be identified in the comparison. The bias is caused by our broad H $\alpha$  selection. The selection is based on the high velocity H $\alpha$  line wing over the wavelength range from 6500 to 6530 Å (i.e., blueward of [NII]  $\lambda 6548$  line) in the rest frame, which naturally results in a significant loss of the objects with small  $\text{FWHM}_{\text{H}\alpha} \lesssim 2000 \text{ km s}^{-1}$ . A similar comparison is shown in the right panel for the calculated  $L/L_{\text{Edd}}$ . Compared with the type I AGNs, the  $L/L_{\text{Edd}}$  distribution of the partially obscured AGNs is systematically shifted to low  $L/L_{\text{Edd}}$  end by an amount of  $\sim 1.0$  dex, although both distributions have roughly identical dynamical range of  $\sim 2.0$  dex. This systematical shift could be explained by the combination of the underestimate of  $L_{\text{H}\alpha}$  and the selection bias of broad H $\alpha$  line width.

### 5.2. Influence of Removal of AGN's Continuum

Comparing with our previous studies, the current measurement of  $D_n(4000)$  index is improved by subtracting an underlying AGN's continuum from the observed spectrum according to the broad H $\alpha$  emission. As stated in Section 3.1, there is an uncertainty for the moved powerlaw continuum due to the uncertainties of reddening and obscuration and the intrinsic scatter of the powerlaw index. We have demonstrated that the measured  $D_n(4000)$  is more sensitive to reddening factor  $\beta$  than to powerlaw index. A Monte-Carlo simulation with 1,000 random experiments is then performed to quantitatively examine the effect on the  $L/L_{\text{Edd}}-D_n(4000)$  correlation caused by the uncertainty of removed powerlaw continuum level. For each object, a random  $D_n(4000)$  is produced by a random sampling of  $\beta$  in the range from 1 to 2. A Spearman rank-order test is then performed for each of the 1,000 random samples. Figure 10 displays the distribution of the simulated correlation coefficient  $r_s$ . The distribution has a mean value of  $\bar{r}_s = -0.604$  and a standard deviation of  $5.0 \times 10^{-3}$ . the simulation indicates that the relationship between  $L/L_{\text{Edd}}$  and  $D_n(4000)$  is not sensitive to the uncertainty of the amplitude of the used powerlaw<sup>10</sup>, although the relationship can be slightly degraded by the uncertainty of the level of the removed powerlaw continuum.

<sup>9</sup>The adopted bolometric correction coefficient is 9 in the current study, and is 9.8 in Greene & Ho (2007).

<sup>10</sup>In the 1,000 experiments, all the calculated probabilities that the two parameters are not correlated are  $\sim 10^{-27}$ .

### 5.3. Feedback in Co-evolution of AGNs and Their Host Galaxies

The relationship between  $L/L_{\text{Edd}}$  and stellar population age of host galaxy has been established by different approaches in past decade. This relationship allows us to establish a co-evolution scenario in which AGNs evolve from a high- $L/L_{\text{Edd}}$  state to a low- $L/L_{\text{Edd}}$  state as the circumnuclear stellar population continually ages. In a wide range of SMBH masses, the majority of local SMBH growth is found to occur not only in the high accretion phase but also in the galaxies with young stellar populations and with ongoing or recent star formations (Goulding et al. 2010; Heckman & Kauffmann 2006 and references therein). Wang et al. (2006) reported a relation between the EI space and middle-far-infrared color  $\alpha(60, 25)$  by performing a PCA analysis on a sample of *IRAS*-selected Seyfert 1.5 galaxies. This relation naturally indicates a relation between  $L/L_{\text{Edd}}$  and host galaxy stellar population, both because the EI space is commonly accepted to be driven by  $L/L_{\text{Edd}}$  (e.g., Boroson 2002) and because the color  $\alpha(60, 25)$  addresses the relative importance of AGN activity and starburst activity. A direct correlation between  $L/L_{\text{Edd}}$  and host stellar population age is established either by using  $L([\text{OIII}])/\sigma_*^4$  as a proxy of  $L/L_{\text{Edd}}$  in type II AGNs (e.g., Kewley et al. 2006; Wild et al. 2007; Kauffmann et al. 2007) or by estimating  $L/L_{\text{Edd}}$  directly from the Balmer broad lines in partially obscured AGNs (Wang et al. 2008, 2010, and this paper). The role of  $L/L_{\text{Edd}}$  in the coevolution issue is additionally revealed from AGN's hard X-ray emission, basing upon an identified correlation between AGN's hard X-ray spectral index and stellar population age of the host galaxy (Wang et al. 2013).

The evolutionary scenario mentioned above describes how AGNs (strictly speaking, which parameters of AGNs) co-evolve with their host galaxies. This phenomenological scenario, however, does not involve the background physical process that produces a self-regulated growth of SMBH mass and host galaxy star formation. One can see from our statistical study that the feedback is a potential “bridge” that links and regulates the growth of SMBH and host galaxy star formation. According to the aforementioned results, a strong AGN-driven feedback is required for an AGN in its early gas-rich phase with both rapid SMBH growth (i.e., high  $L/L_{\text{Edd}}$ ) and young host stellar population, although the physical process that drives the outflow is still an open question. In contrast, a weak feedback is sufficient to regulate SMBH mass growth and host star formation in the late gas-poor phase. The available models include AGN's wind (e.g., Crenshaw et al. 2003; Pounds et al. 2003; Ganguly et al. 2007; Reeves et al. 2009; Dunn et al. 2010; Tombesi et al. 2012), radiation pressure (e.g., Alexander et al. 2010) and radio jets (e.g., Rosario et al. 2010). In the current sample, the non-detection of the connection between radio emission and [OIII] line profile (see Section 5.4) allows us to believe that the radiation pressure is probably the initial driver of the outflows. Matsuoka (2012) recently identified a deficit of extended emission-line region in the AGNs with high  $L/L_{\text{Edd}}$ . The deficit could be explained by the AGN's feedback that blows the gas around SMBH away. Moreover, the spectroscopic observations using integral-field unit suggest the similar signatures of outflow in high-redshift galaxies/quasars (e.g., Nesvadba et al. 2008; Cano-Diaz et al. 2012; Harrison et al. 2012), where the outflow from AGN is predicted to be much stronger than in local universe according to the model of cosmic galaxy formation (see a more extended discussion on this issue at the end of this subsection).

The revealed dependence between feedback and AGN-host co-evolution provides an evidence that supports the hypothesis that the host star formation is regulated by SMBH growth through the information provided by AGN-driven feedback. Both AGN-suppressed and AGN-induced host star formation have been proposed in past decades, although we can not say which one occurs in AGNs based on our current results. A commonly accepted mechanism that the feedback works is that the feedback from central AGN sweeps out circumnuclear gas, which suppresses star

formation and results in a self-regulated SMBH growth and host star formation in both galaxies merger and secular evolution scenarios (e.g., Alexander & Hickox 2012; Fabian 2012; Kormendy & Ho 2012;). In the color versus absolute magnitude diagram, there is an excess of AGNs in the “green valley” between the blue cloud and red sequence (e.g., Sanchez et al. 2004; Nandra et al. 2007; Schawinski et al. 2009; Treister et al. 2009; Georgakakis et al. 2009; Cisternas et al. 2011; Mullaney et al. 2012; Rosario et al. 2012). The excess implies that AGNs are at a transition from the blue cloud to the red sequence, which is likely resulted from a suppression of star formation due to the feedback from AGNs<sup>11</sup> (e.g., Nandra et al. 2007; Hickox et al. 2009; Hopkins & Elvis 2010). Zubovas et al. (2013 and references therein) recently performed a study on positive feedback through well-resolved numerical simulations of AGN’s feedback process. At early gas-rich phase, the energy-driven feedback compresses the cold gas in host galaxy into dense shells and clumps, which triggers star formation if the shocked gas cools rapidly. A negative feedback that quenches the star formation, however, occurs at late gas-poor phase.

The model in King (2003, 2005) indicates that the  $M_{\text{BH}} - \sigma_{\star}$  relation is established through the momentum-driven flow with a mildly relativistic velocity of  $v_w \sim \eta c$ , where  $\eta \sim 0.1$  is the accretion efficiency. However, a energy-driven outflow at large scale is expected after the  $M_{\text{BH}} - \sigma_{\star}$  relationships established. The outflow velocity is  $v_{\text{out}} \simeq 925 \sigma_{200}^{2/3} (\lambda_{\text{Edd}} f_c / f_g)^{1/3} \text{km s}^{-1}$  (King et al. 2011, Zubovas & King 2012), where  $\sigma_{200}$  is the velocity dispersion in bulge,  $\lambda_{\text{Edd}}$  Eddington ratio of central SMBH,  $f_c = 0.16$  the cosmology value of the baryon-to-dark-matter density fraction, and  $f_g$  the gas fraction in bulge that is of the same order of  $f_c$ . In the current sample, we have the averaged values of  $\overline{\sigma_{\star}} \approx 100 \text{km s}^{-1}$  and  $\overline{\lambda_{\text{Edd}}} \approx 0.04$ . With these values, the outflow velocity at large scale is expected to be  $v_{\text{out}} \sim 200 \text{km s}^{-1}$ , which is close to the velocity shift measured from the [OIII] emission lines.

Large-scale outflow is expected to be strong in high redshift ( $z \sim 2$ ) AGNs where the peaks of both AGN’s activity and star formation occur roughly coincident (e.g., Ishibashi et al. 2013). Searching for the relationship between the strength of AGN’s feedback and effect on host properties in high- $z$  universe is important for understanding the impact of the feedback on the galaxy formation and evolution. In spite of the debates (e.g., Santini et al. 2012; Harrison et al. 2012), Page et al. (2012) claims a suppressed star formation in powerful AGNs in the redshift range from  $z = 1$  to 3 basing upon the Herschel SPIRE observations in sub-millimeter.

#### 5.4. Radio Emission And [OIII] Line Profile

The interaction between radio jet and ISM is another possible mechanism that drives outflow in galactic-scale (e.g., Holt et al. 2008; Nesvadba et al. 2008; Guillard et al. 2012). An outflow of cold, neutral gas due to jet-ISM interaction is identified by many observations (e.g., Morganti et al. 2005, 2007; Holt et al. 2011; Mahony et al. 2013). There is an alignment between radio jet and structure in (extended) NLR in many objects (e.g., Whittle & Wilson 2004; Rosario et al. 2010). Strong blue wings of [OIII] $\lambda 5007$  lines have been identified by Brotherton (1996) in a sample of radio-loud quasars. The [OIII] line width is found to be correlated with radio luminosity at 1.4GHz ( $L_{1.4\text{GHz}}$ ) for flat-spectrum radio galaxies in early studies (e.g., Heckman et al. 1984; Whittle 1985). By using a large sample of AGNs (both type I and type II) from SDSS,

<sup>11</sup>Recent direct measurements of star formation through [OII] emission line and infrared emission indicate that these AGNs are in reddened star-forming galaxies, rather than in a transition phase (e.g., Silverman et al. 2009; Mullaney et al. 2012; Rosario et al. 2013). Xue et al. (2010) indicates that AGN hosts and non-AGN galaxies occupy the same region in the color-magnitude diagram by using mass-matched samples.

Mullaney et al. (2013) claimed that the [OIII] line width is more strongly related to  $L_{1.4\text{GHz}}$  than the other AGN's parameters.

The partially obscured AGNs listed in the current sample are cross-matched with the FIRST survey catalog (Becker et al. 2003) to examine the connection between their radio emission and [OIII] line profiles. The cross-match returns 69 Seyfert galaxies and 26 composite galaxies with detected radio flux exceeding the FIRST limiting flux density ( $5\sigma$ ) of 1mJy. Their radio fluxes range from 1.0 to 734mJy. All these objects have a radio emission with  $S/N > 3$ . An underlying contribution from host starburst is a possible explanation of the high fraction of radio detection in current sample ( $\sim 45\%$ ) than in typical type-I AGNs ( $\sim 10\%$ , e.g., Rafter et al. 2009; Mullaney et al. 2013). The most radio-luminous starburst galaxies ( $z = 0.01 - 0.05$ ) have a radio luminosity of  $\log P_{5\text{GHz}} = 22.3 - 23.4$  (Smith et al. 1998). The high detection rate could be alternatively attributed to our sample selection criterion, which excludes the majority of less luminous AGNs, such as LINERs, with faint [OIII] line emission. The luminosity at 1.4GHz is calculated from  $L_{1.4\text{GHz}} = 4\pi d_L^2 f_\nu (1+z)^{-\alpha-1}$ , where  $f_\nu$  is the integrated flux density at 1.4GHz,  $d_L$  is the luminosity distance, and  $\alpha = -0.8$  (e.g., Ker et al. 2012) is the spectral slope defined as  $f_\nu \propto \nu^\alpha$ .  $L_{1.4\text{GHz}}$  is plotted against  $\xi_3$  and  $\Delta\nu$  in the left and right panel in Figure 11, respectively. The calculated radio luminosity ranges from  $10^{20}$  to  $10^{25} \text{ W Hz}^{-1}$ . One can see from the figure that there is no evident connection between the radio emission and the [OIII] line profile asymmetry and bulk velocity blueshift in the current sample. The strongest radio emission (i.e.,  $L_{1.4\text{GHz}} > 10^{24} \text{ W Hz}^{-1}$ ) in fact occurs in a few of objects with nearly Gaussian profile and small velocity shift with  $-100\text{km s}^{-1}$  at most. The lack of numbers in our partially obscured AGN sample (95 vs. 1,988) is a possible explanation for none detection of the influence by radio emission seen in Mullaney et al. (2013).

##### 5.5. Comparison with Type II AGNs

The spectral analysis in this study allows us to compare the [OIII] line profile between the partially obscured Seyfert galaxies and the Seyfert 2 galaxies that are studied in Wang et al. (2011). The distributions of line width,  $\xi_3$  and  $\Delta\nu$  are compared in Figure 12. The three panels show that the partially obscured AGNs tend to have wider [OIII] line, stronger blue asymmetry and larger bulk velocity blueshift than do the Seyfert 2 galaxies.

These results are in agreement with previous studies, and are easily understood in the context of the AGN's unified model (e.g., Antonucci 1993). Vaona et al. (2012) performed a comprehensive comparison of narrow emission line between Seyfert 2 galaxies and intermediate-type Seyfert galaxies. The authors identified a higher percentage of strong [OIII] line blue asymmetry and large line width in the intermediate-type Seyfert galaxies than in the Seyfert 2 galaxies. A similar conclusions are recently obtained in a comparison between type I and type II Seyfert galaxies in Mullaney et al. (2013). The [OIII] line asymmetry and bulk velocity blueshift are widely used to characterize AGN's outflows that are initially launched from accretion disc or dusty torus (e.g. Heckman et al. 1981; Barth et al. 2008; Nesvadba et al. 2008; Greene et al. 2011). In the context of the unified model, the observed properties of the outflow inferred from [OIII] emission depend on the orientation of the AGN's ionization cone with respect to the line-of-sight of an observer. A more asymmetrical [OIII] line profile and a larger bulk velocity are expected in partially obscured AGNs than in Seyfert 2 galaxies if the outflow is along the axis perpendicular to the plane of torus.

A majority difference between the current study and Wang et al. (2011) is the method used to estimate  $L/L_{\text{Edd}}$ .  $L/L_{\text{Edd}}$  is obtained through [OIII] line luminosity and stellar velocity dispersion in Wang et al. (2011), and through broad H $\alpha$  emission in this paper. Figure 13 compares the

different methods in the current partially obscured AGN sample. The left panel shows a tight correlation between the luminosities of the two emission lines. One can see clearly a large scatter, a systematical offset and different dynamical ranges when the Eddington ratios estimated from  $H\alpha$  ( $L/L_{\text{Edd}}$ ) and [OIII] lines ( $\lambda_{\text{Edd}}$ ) are compared with each other in the middle panel. Our examination indicates that the large scatter and the systematic are mainly caused by the poor relationship between the  $M_{\text{BH}}$  determined by  $H\alpha$  line and stellar velocity dispersion.

## 6. CONCLUSION

The role of feedback in the AGN-host coevolution issue is re-studied here by focusing on the [OIII] emission line profile in partially obscured AGNs selected from SDSS DR7. The broad  $H\alpha$  emission lines enable us to 1) directly determine the AGN's accretion properties; 2) subtract an underlying AGN's continuum from the observed spectrum. With these improvements, our analysis indicates (confirms) that the AGNs associated with young stellar population tend to be of large  $L/L_{\text{Edd}}$ , strong [OIII] blue asymmetry and large [OIII] bulk velocity blueshift, which implies that the feedback from central AGN plays an important role in linking as self-regulated SMBH growth and host star formation.

### *Acknowledgments*

We thank the anonymous referee for his/her helpful suggestions for improving the manuscript. This study uses the SDSS archive data that was created and distributed by the Alfred P. Sloan Foundation. The study is supported by the National Basic Research Program of China (973-program, grant No. 2014CB845800) and by the National Science Foundation of China under grant 11473036.

## References

- Abazajian, K. N., Adelman-McCarthy, J. K., Agueros, M. A., et al. 2009, *ApJS*, 182, 543  
Aird, J., et al. 2010, *MNRAS*, 401, 2531  
Alatalo, K., et al. 2011, *ApJ*, 735, 88  
Alexander, D. M., & Hickox, R. C. 2012, *NewAR*, 56, 93  
Aller, M. C., & Richstone, D. O. 2007, *ApJ*, 665, 120  
Antonucci, R. R. J. 1993, *ARA&A*, 31, 473  
Aoki, K., Kawaguchi, T., & Ohta, K. 2005, *ApJ*, 618, 601  
Assef, R. J., et al. 2011, *ApJ*, 728, 56  
Balogh, M. L., et al. 1999, *ApJ*, 527, 54  
Baldwin, J. A., Phillips, M. M., & Terlevich, R. 1981, *PASP*, 93, 5  
Barth, A. J., Greene, J. E., & Ho, L. C. 2008, *AJ*, 136, 1179  
Becker, R. H., Helfand, D. J., White, R. L., Gregg, M. D., & Laurent-Muehleisen, S. A. 2003, *VizieR Online Data Catalog*, 8071, 0  
Bentz, M. C., Peterson, B. M., Pogge, R. W., Vestergaard, M., & Onken, C. A. 2006, *ApJ*, 644, 133  
Bian, W. H., Yuan, Q. R., & Zhao, Y. H. 2005, *MNRAS*, 364, 187  
Binney, J., & Merrifield, M. 1998, *Galactic Astronomy* (Princeton, NJ: Princeton Univ. Press)  
Boroson, T. A. 2002, *ApJ*, 565, 78  
Boroson, T. A. 2005, *AJ*, 130, 381  
Brotherton, M. S. 1996, *ApJS*, 102, 1  
Bruzual, A. G. 1983, *ApJ*, 273, 105  
Bruzual, G., & Charlot, S. 2003, *MNRAS*, 344, 100  
Cano-Diaz, M., Maiolino, R., Marconi, A., Netzer, H., Shemmer, O., & Cresci, G. 2012, *A&A*, 537, L8  
Cid Fernandes, R. Jr., & Terlevich, R. 1995, *MNRAS*, 272, 423  
Cid Fernandes, R., Gu, Q., Melnick, J., Terlevich, E., Terlevich, R., Kunth, D., Rodrigues Lacerda, R., & Joguet, B. 2004, *MNRAS*, 355, 273  
Ciotti, L., & Ostriker, J. P. 2007, 665, 1038

Cisternas, M., et al. 2011, *ApJ*, 726, 57

Crenshaw, D. M., et al. 2003, *ApJ*, 594, 116

Croom, S. M., Smith, R. J., Boyle, B. J., Shanks, T., Miller, L., Outram, P. J., & Loaring, N. S. 2004, *MNRAS*, 349, 1379

Croton, D. J., Springel, V., White, S. D. M., et al. 2006, *MNRAS*, 365, 1

Di Matteo, P., Combes, F., Melchior, A.-L., & Semelin, B. 2007, *A&A*, 468, 61

Di Matteo, T., Springel, V., & Hernquist, L. 2005, *Nature*, 433, 604

Dehnen, W., & King, A. 2013, *ApJL*, 777, 28

Dunn, J. P., et al. 2010, *ApJ*, 709, 611

Fabian, A. C. 1999, *MNRAS*, 308, L39

Fabian, A. C. 2012, *ARA&A*, 50, 455

Ferrarese, L., & Ford, H. 2005, *SSR*, 116, 523

Feruglio, C., Maiolino, R., Piconcelli, E., Menci, N., Aussel, H., Lamastra, A., & Fiore, F. 2010, *A&A*, 518, L155

Fischer, T. C., Crenshaw, D. M., Kraemer, S. B., & Schmitt, H. R. 2013, *ApJS*, 209, 1

Francis, P. J., Hewett, P. C., Foltz, C. B., & Chaffee, F. H. 1992, *ApJ*, 398, 476

Fu, H., & Stockton, A. 2009, *ApJ*, 690, 953

Ganguly, R., Brotherton, M. S., Cales, S., Scoggins, B., Shang, Z., & Vestergaard, M. 2007, *ApJ*, 665, 990

Gebhardt, K. et al. 2000, *ApJL*, 539, 13

Georgakakis, A., Clements, D. L., Bendo, G., Rowan-Robinson, M., Nandra, K., & Brotherton, M. S. 2009, *MNRAS*, 394, 533

Goulding, A. D., Alexander, D. M., Lehmer, B. D., & Mullaney, J. R. 2010, *MNRAS*, 406, 597

Granato, G. L., De Zotti, G., Silva, L., Bressan, A., & Danese, L. 2004, *ApJ*, 600, 580

Greene, J. E., & Ho, L. C. 2005, *ApJ*, 630, 122

Greene, J. E., & Ho, L. C. 2007, *ApJ*, 670, 92

Greene, J. E., Zakamska, N. L., Ho, L. C., & Barth, A. J. 2011, *ApJ*, 732, 9

Guillard, P., et al. 2012, *ApJ*, 747, 95

Gultekin, K., et al. 2009, *ApJ*, 698, 198

Haehnelt, M. G., Natarajan, P., Rees, M. J. 1998, *MNRAS*, 300, 817

Hao, L., et al. 2005, *AJ*, 129, 1795

Haring, N., & Rix, H. W. 2004, *ApJL*, 604, 89

Harrison, C. M., et al. 2012, 426, 1073

Hasinger, G., Miyaji, T., & Schmidt, M. 2005, *A&A*, 441, 417

Heckman, T. M., & Kauffmann, G. 2006, *NewAR*, 50, 677

Heckman, T. M., Miley, G. K., & Green, R. F. 1984, *ApJ*, 281, 525

Heckman, T. M., Miley, G. K., van Breugel, W. J. M., & Butcher, H. R. 1981, *ApJ*, 247, 403

Hickox, R. C., et al. 2009, *ApJ*, 696, 891

Hirschmann, M., Dolag, K., Saro, A., Borgani, S., & Burkert, A. 2013, *astro-ph/arXiv1308.0333*

Holt, J., Tadhunter, C. N., & Morganti, R. 2008, *MNRAS*, 387, 639

Holt, J., Tadhunter, C. N., Morganti, R., & Emonts, B. H. C. 2011, *MNRAS*, 410, 1527

Hopkins, P. F., Bundy, K., Hernquist, L., & Ellis, R. S. 2007, *ApJ*, 659, 976

Hopkins, P. F., Cox, T. J., Keres, D., & Hernquist, L. 2008, *ApJS*, 175, 390

Hopkins, P. F., & Elvis, M. 2010, *MNRAS*, 401, 7

Ishibashi, W., Fabian, A. C., & Canning, R. E. A. 2013, *MNRAS*, 431, 2350

Kaspi, S., Smith, P. S., Netzer, H., Maoz, D., Jannuzi, B. T., & Givon, U. 2000, *ApJ*, 533, 631

Kauffmann, G., & Haehnelt, M. 2000, *MNRAS*, 311, 576

Kauffmann, G., & Heckman, T. M. 2009, *MNRAS*, 397, 135

Kauffmann, G., Heckman, T. M., White, S. D. M., et al. 2003, *MNRAS*, 341, 33

Kauffmann, G., et al. 2007, *ApJS*, 173, 357

Ker, L. M., Best, P. N., Rigby, E. E., Rttgering, H. J. A., & Gendre, M. A. 2012, *MNRAS*, 420, 2644

Kewley, L. J., Dopita, M. A., Sutherland, R. S., Heisler, C. A., & Trevena, J. 2001, *ApJ*, 556, 121

Kewley, L. J., Groves, B., Kauffmann, G., & Heckman, T. 2006, *MNRAS*, 372, 961

Khalatyan, A., Cattaneo, A., Schramm, M., Gottlber, S., Steinmetz, M., & Wisotzki, L. 2008, *MNRAS*, 387, 13

King, A. 2005, *ApJL*, 596, 27

King, A. 2005, *ApJL*, 635, 121

King, A., Zubovas, K., & Power, C. 2011, *MNRAS*, 415, L6

Kormendy, J. & Ho, L. C. 2013, *ARA&A*, 51, 511

Komossa, S. 2008, *RevMexAA Conf. Ser.*, 32, 86

Komossa, S., & Xu, D. 2007, *ApJ*, 677, 33

Komossa, S., Xu, D., Zhou, H., Storchi-Bergmann, T., & Binette, L. 2008, *ApJ*, 680, 926

Kriss, G. 1994, *Adass*, 3, 43

Magorrian, J., et al. 1998, *AJ*, 115, 2285

Mahony, E. K., Morganti, R., Emonts, B. H. C., Oosterloo, T. A., & Tadhunter, C. 2013, *MNRAS*, 435, L58

Marziani, P., & Sulentic, J. W. 2012, *New Astronomy Review*, 56, 49

Marziani, P., Sulentic, J. W., Zamanov, R., et al. 2003, *ApJS*, 145, 199

Mathur, S. 2000, *MNRAS*, 314, L17

Matsuoka, Y. 2012, *ApJ*, 2012, 750, 54

McLure, R. J., & Dunlop, J. S. 2002, *MNRAS*, 331, 795

Merritt, D., & Ferrarese, L. 2001, *MNRAS*, 320, L30

Menci, N., Fiore, F., Puccetti, S., & Cavaliere, A. 2008, *ApJ*, 686, 219

Morganti, R., Holt, J., Saripalli, L., Oosterloo, T. A., & Tadhunter, C. N. 2007, *A&A*, 476, 735

Morganti, R., Oosterloo, T. A., Tadhunter, C. N., van Moorsel, G., & Emonts, B. 2005, *A&A*, 439, 521

Mullaney, J. R., et al. 2012, *ApJL*, 753, 30

Mullaney, J. R., Alexander, D. M., Fine, S., Goulding, A. D., Harrison, C. M., & Hickox, R. C. 2013, *MNRAS*, 433, 622

Murray, N., Quataert, E., & Thompson, T. A. 2005, *ApJ*, 618, 569

Nandra, K., Laird, E. S., & Steidel, C. C. 2005, *MNRAS*, 360, L39

Nandra, K., et al. 2007, *ApJL*, 660, 11

Nesvadba, N. P. H., Lehnert, M. D., De Breuck, C., Gilbert, A. M., & van Breugel, W. 2008, *A&A*, 491, 407

Page, M. J. et al., 2012, *Nature*, 485, 213

Pounds, K. A., King, A. R., Page, K. L., & O'Brien, P. T. 2003, *MNRAS*, 346, 1025

Rafter, S. E., Crenshaw, D. M., & Wiita, P. J. 2009, *AJ*, 137, 42

Reeves, J. N., Sambruna, R. M., Braitto, V., & Eracleous, M. 2009, *ApJL*, 702, 187

Rosario, D. J., et al. 2012, *A&A*, 535, 45

Rosario, D. J., et al. 2013, *ApJ*, 763, 59

Rosario, D. J., Shields, G. A., Taylor, G. B., Salviander, S., & Smith, K. L. 2010, *ApJ*, 716, 131

Rupke, D. S. N., & Veilleux, S. 2011, *ApJL*, 729, 21

Sanchez, S. F., et al. 2004, *ApJ*, 641, 586

Santini, P., et al. 2012, *A&A*, 540, 109

Schawinski, K., Thomas, D., Sarzi, M., Maraston, C., Kaviraj, S., Joo, S., Yi, S. K., & Silk, J. 2007, *MNRAS*, 382, 1415

Schawinski, K., Virani, S., Simmons, B., Urry, C. M., Treister, E., Kaviraj, S., & Kushkuley, B. 2009, *ApJL*, 692, 19

Shankar, F., Bernardi, M., & Haiman, Z. 2009, *ApJS*, 694, 867

Silk, J., & Rees, M. J. 1998, *A&A*, 331, L1

Silverman, J. D., et al. 2008, *ApJS*, 679, 118

Silverman, J. D., et al. 2009, *ApJS*, 696, 396

Spergel, D. N., et al. 2003, *ApJS*, 148, 175

Springel, V., White, S. D. M., Jenkins, A., et al. 2005, *Nature*, 435, 629

Somerville, R. S., Hopkins, P. F., Cox, T. J., Robertson, B. E., & Hernquist, L. 2008, *MNRAS*, 391, 481

Stasinska, G., Cid Fernandes, R., Mateus, A., Sodre, L., & Asari, N. V. 2006, *MNRAS*, 371, 972

Storchi-Bergmann, T., Raimann, D., Bica, E. L. D., & Fraquelli, H. A. 2000, *ApJ*, 544, 747

Tombesi, F., Cappi, M., Reeves, J. N., & Braitto, V. 2012, *MNRAS*, 422, L1

Tremaine, S., Gebhardt, K., Bender, R., et al. 2002, *ApJ*, 574, 740

Treister, E., et al. 2009, *ApJ*, 706, 535

Ueda, Y., Akiyama, M., Ohta, K., & Miyaji, T. 2003, *ApJ*, 598, 886

Vanden Berk, D. E., et al. 2001, *AJ*, 122, 594

Vaona, L., Ciroi, S., Di Mille, F., Cracco, V., La Mura, G., & Rafanelli, P. 2012, *MNRAS*, 427, 1266

Veilleux, S., & Osterbrock, D. E. 1987, *ApJS*, 63, 295

Veron-Cetty, M.-P., Veron, P., & Goncalves, A. C. 2001, *A&A*, 372, 730

Wang, J., & Wei, J. Y. 2008, *ApJ*, 679, 86

Wang, J., & Wei, J. Y. 2010, *ApJ*, 719, 1157

Wang, J., Mao, Y. F., & Wei, J. Y. 2011, *ApJ*, 741, 50

Wang, J., Wei, J. Y., & He, X. T. 2006, *ApJ*, 638, 106

Wang, J., Zhou, X. L., & Wei, J. Y. 2013, *ApJ*, 768, 176

Westmoquette, M. S., Smith, L. J., & Gallagher, J. S. III. 2011, *MNRAS*, 414, 3719

Whittle, M. 1985, *MNRAS*, 213, 33

Whittle, M., & Wilson, A. S. 2004, *AJ*, 127, 606

Wild, V., Heckman, T. M., & Charlot, S. 2010, *MNRAS*, 405, 933

Wild, V., Kauffmann, G., Heckman, T., et al. 2007, *MNRAS*, 381, 543

Woo, J. H., et al. 2010, *ApJ*, 716, 269

Xu, D. W., & Komossa, S. 2009, *ApJ*, 705, 20

Xue, Y. Q., et al. 2010, *ApJ*, 720, 368

- Zamanov, R., Marziani, P., Sulentic, J. W., et al. 2002, *ApJ*, 576, 9  
Zhang, K., Wang, T., Gaskell, C. M., & Dong, X. 2013, *ApJ*, 762, 51  
Zhou, H. Y., Wang, T. G., Yuan, W. M., Lu, H. L., Dong, X. B., Wang, J. X., & Lu, Y. J. 2006, *ApJS*, 166, 128  
Zubovas, K., & King, A. R. 2012, 426, 2751  
Zubovas, K., Nayakshin, S., King, A., & Wilkinson, M. 2013, *MNRAS*, 433, 3079



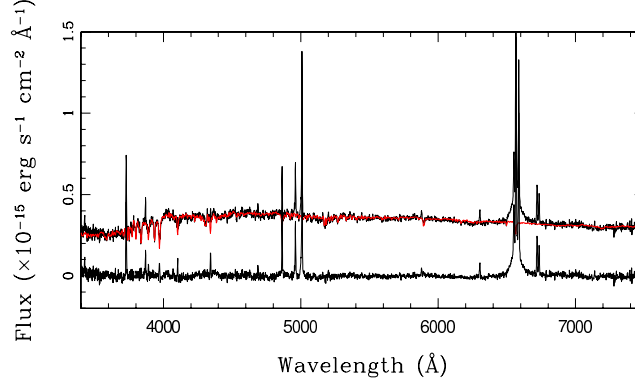


Figure 1: An illustration of the continuum modeling and subtraction for a typical case of SDSS J095156.71+023602.0. The raw spectrum and emission-line isolated spectrum are shown by the two black curves. The red curve presents the modeled continuum by a linear sum of the seven eigenspectra built from Bruzual & Charlot (2003), in which the contamination by the AGN's continuum is not removed.

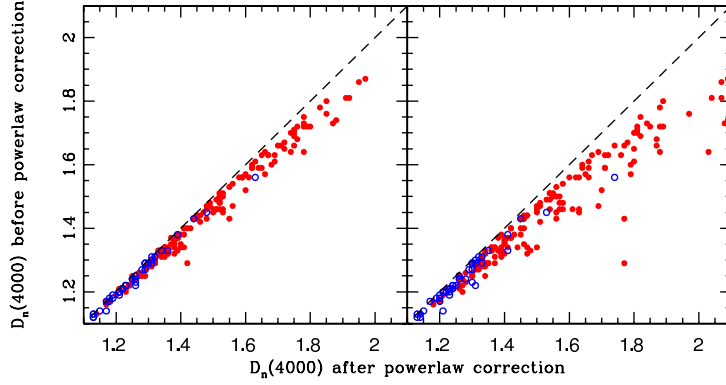


Figure 2: A comparison between the  $D_n(4000)$  measurements after the correction of an underlying AGN's continuum and the ones without the correction. *Left panel:* for  $\beta = 1$ ; *Right panel:* for  $\beta = 2$ . See text for the definition of the parameter  $\beta$ . The Seyfert galaxies and composite galaxies are shown by the red-solid and blue-open circles, respectively.

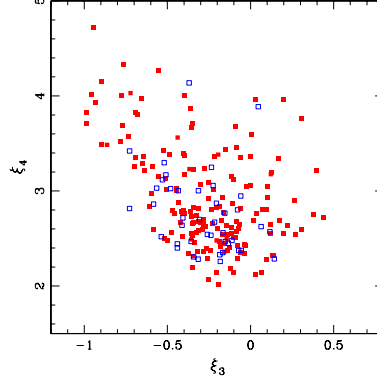


Figure 3: The [OIII] $\lambda$ 5007 line parameter  $\xi_4$  (kurtosis) is plotted against  $\xi_3$  (skewness) for the partially obscured AGNs. The Seyfert galaxies and composite galaxies are shown by the red-solid and blue-open squares, respectively.

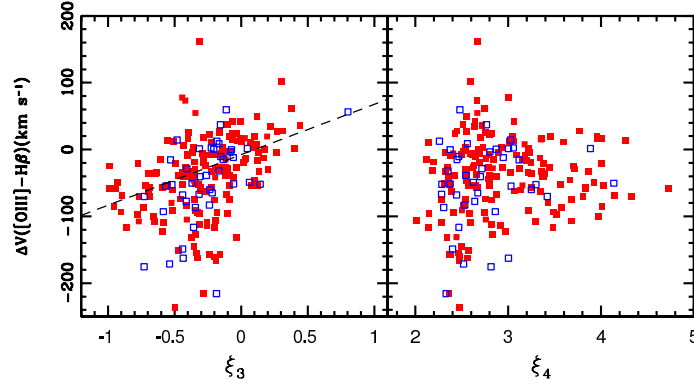


Figure 4: Bulk velocity shift  $\Delta v$  of [OIII] $\lambda$ 5007 line is plotted as a function of the parameters  $\xi_3$  (left panel) and  $\xi_4$  (right panel) for the partially obscured AGNs. The symbols are the same as in Figure 3. The dotted line in the left panel shows the best fit of the relationship.

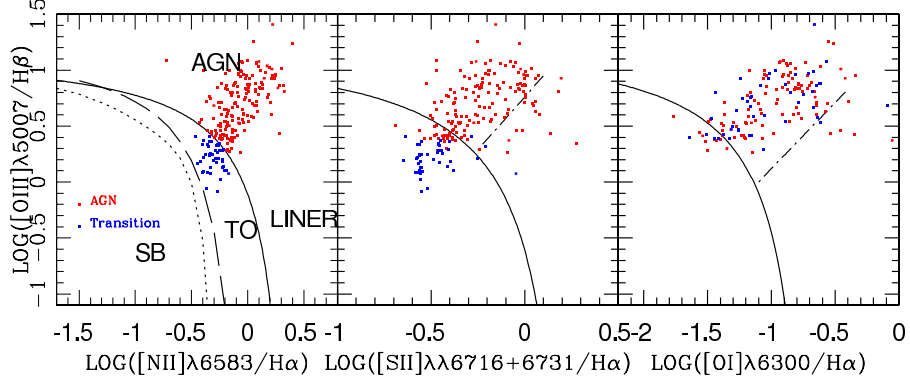


Figure 5: Three BPT diagnostic diagrams for the partially obscured AGNs. The symbols are the same as in Figure 3. The solid lines in all the three panels show the theoretical demarcation lines separating AGNs from star-forming galaxies proposed by Kewley et al. (2001). In the left panel, the long-dashed line shows the empirical line proposed in Kauffmann et al. (2003), and the short-dashed line the theoretical line given in Stasinska et al. (2006). Both lines are used to separate “pure” star-forming galaxies. The dashed-dotted lines in the middle and right panels mark the empirical demarcation lines separating Seyfert galaxies and LINERs proposed in Kewley et al. (2006).

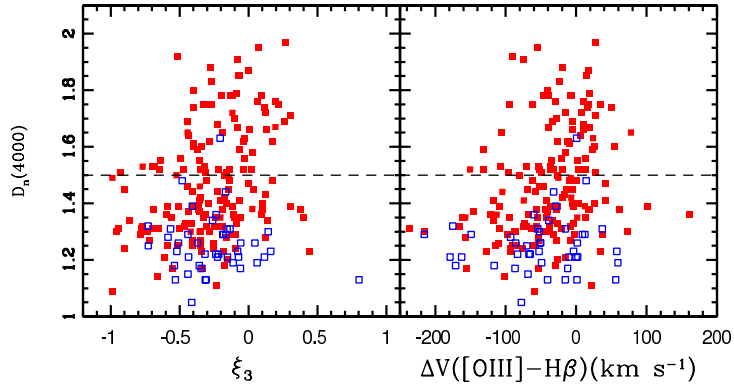


Figure 6: Stellar population ages (i.e., the  $D_n(4000)$  index) plotted against the  $[\text{OIII}]\lambda 5007$  line shape parameter  $\xi_3$  and bulk velocity shift  $\Delta v$  for the partially obscured AGNs. The symbols are the same as in Figure 3. The horizontal dashed lines in both panels mark the value of  $D_n(4000) = 1.5$  that is used to separate the sample into two parts (i.e., with young and old stellar population). The two sub-samples show a significant difference in the distributions of their  $[\text{OIII}]\lambda 5007$  line shape and bulk velocity shift. AGNs with old host stellar populations are associated with both symmetric  $[\text{OIII}]\lambda 5007$  line profile and small bulk velocity shift ( $> -100 \text{ km s}^{-1}$ ). On the contrary, significant blue wings and bulk blueshift velocities can be only identified in the AGNs with young stellar populations.

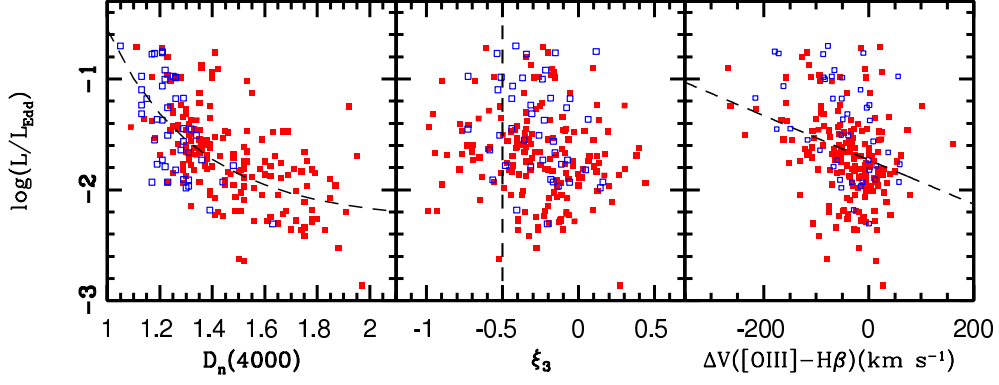


Figure 7: *Left panel:*  $L/L_{\text{Edd}}$  plotted as a function of stellar population age index  $D_n(4000)$ . The best fit nonlinear relationship (see Eq. 5 in the main text) is over plotted by the dash line. *Middle and right panels:*  $L/L_{\text{Edd}}$  plotted against  $\xi_3$  and  $\Delta v$ . The vertical dashed line at  $\xi_3 = -0.5$  in the middle panel is used to separate the sample into two sub-samples (see Figure 8). **A best fit by the linear least square regression is shown by the dashed line in the right panel.** The symbols are the same as in Figure 3.

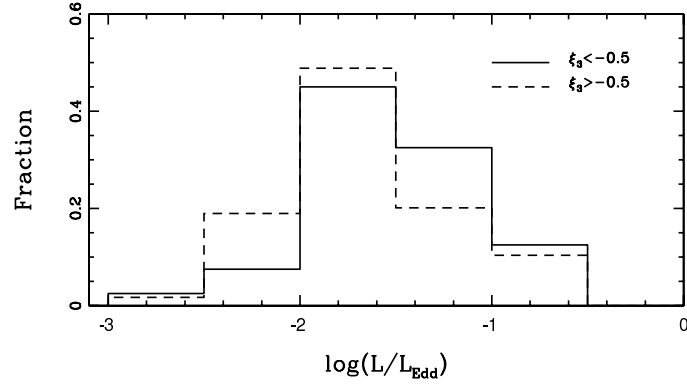


Figure 8: Comparison of the distributions of  $L/L_{\text{Edd}}$  obtained from broad  $\text{H}\alpha$  emission line for the two sub-samples with different  $[\text{OIII}]$  line shape parameter  $\xi_3$ . The solid and dashed lines represent the objects with  $\xi_3 < -0.5$  and  $\xi_3 > -0.5$ , respectively.

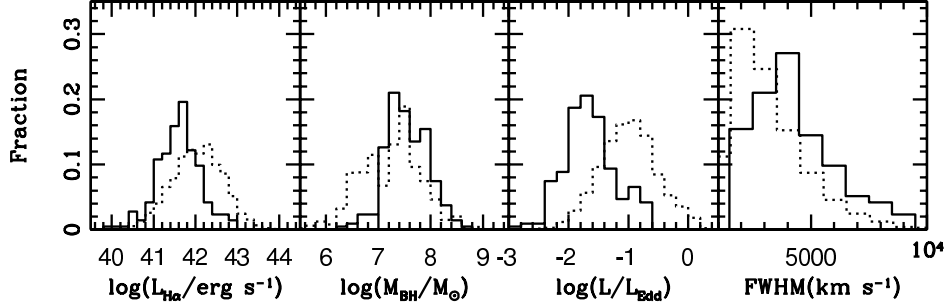


Figure 9: A comparison of the distributions of various parameters between the used partially obscured AGNs (solid line) and the sample of type I AGNs (dotted line) in Greene & Ho (2007). The parameters are luminosity of broad H $\alpha$  emission  $L_{H\alpha}$ , SMBH mass  $M_{BH}$ , Eddington ratio  $L/L_{Edd}$  and H $\alpha$  line width from left to right panels.

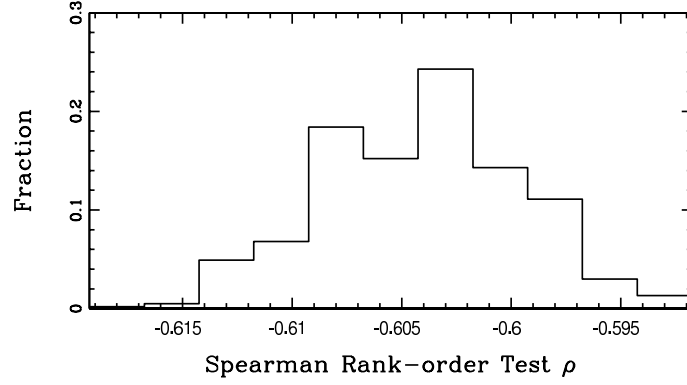


Figure 10: Distribution of the simulated Spearman rank-order test coefficient for the  $L/L_{Edd} - D_n(4000)$  correlation. A Monte-Carlo simulation with 1,000 experiments is carried out by a random sampling of the level of removed AGN's continuum. See text for the details of the simulation.

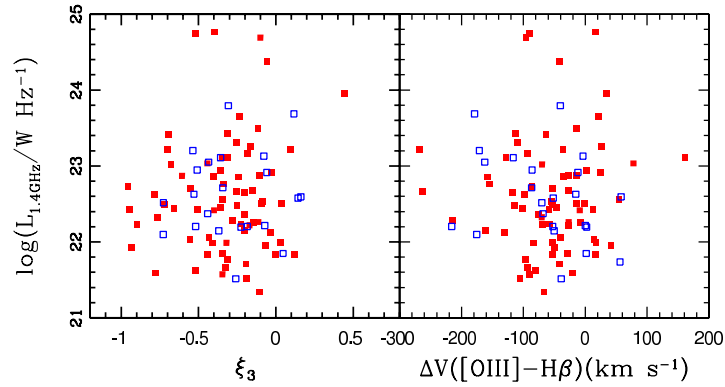


Figure 11: The inferred radio luminosity at 1.4GHz plotted against [OIII] line shape parameter  $\xi_3$  (left panel) and bulk velocity shift  $\Delta v$  (right panel). The symbols are the same as in Figure 3.

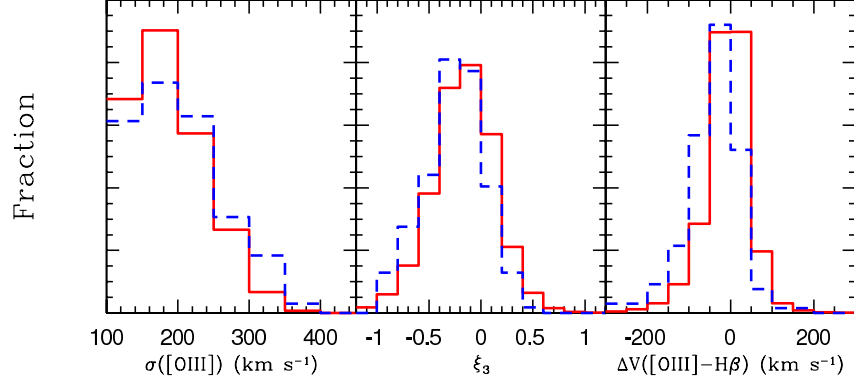


Figure 12: *Left panel*: the distribution of [OIII] $\lambda$ 5007 line width is compared between the partially obscured Seyfert galaxies (blue-dashed line, this paper) and the Seyfert 2 galaxies (red-solid line) studied in Wang et al. (2011). *Middle and right panels*: the same as the left panel but for  $\xi_3$  and  $\Delta\nu$ , respectively.

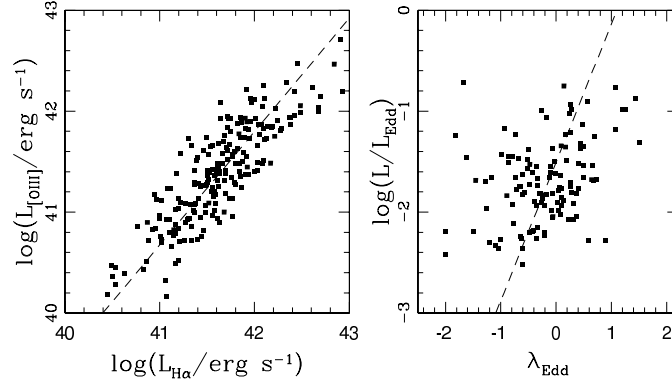


Figure 13: *Left panel*:  $L_{H\alpha}$  versus  $L_{[OIII]}$  for the partially obscured AGNs used in the current study. *Right panel*: Y-axis denotes the  $L/L_{\text{Edd}}$  in logarithm estimated from broad  $H\alpha$ , and X-axis the Eddington ratio  $\lambda_{\text{Edd}} = \log L/L_{\text{Edd}}$  estimated from [OIII] luminosity and stellar velocity dispersion.